
This is an electronic reprint of the original article.
This reprint may differ from the original in pagination and typographic detail.

Westin, Karin; Beniczky, Sándor; Pfeiffer, Christoph; Hämäläinen, Matti; Lundqvist, Daniel
On the clinical utility of on-scalp MEG : A modeling study of epileptic activity source estimation

Published in:
Clinical Neurophysiology

DOI:
[10.1016/j.clinph.2023.10.006](https://doi.org/10.1016/j.clinph.2023.10.006)

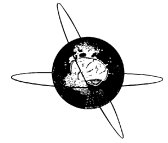
Published: 01/12/2023

Document Version
Publisher's PDF, also known as Version of record

Published under the following license:
CC BY

Please cite the original version:
Westin, K., Beniczky, S., Pfeiffer, C., Hämäläinen, M., & Lundqvist, D. (2023). On the clinical utility of on-scalp MEG : A modeling study of epileptic activity source estimation. *Clinical Neurophysiology*, 156, 143-155.
<https://doi.org/10.1016/j.clinph.2023.10.006>

This material is protected by copyright and other intellectual property rights, and duplication or sale of all or part of any of the repository collections is not permitted, except that material may be duplicated by you for your research use or educational purposes in electronic or print form. You must obtain permission for any other use. Electronic or print copies may not be offered, whether for sale or otherwise to anyone who is not an authorised user.



On the clinical utility of on-scalp MEG: A modeling study of epileptic activity source estimation



Karin Westin^{a,b,*}, Sándor Beniczky^c, Christoph Pfeiffer^a, Matti Hämäläinen^d, Daniel Lundqvist^a

^a Department of Clinical Neuroscience, Karolinska Institutet, Stockholm, Sweden

^b Clinical Neurophysiology, Karolinska University Hospital, Stockholm, Sweden

^c Department of Clinical Neurophysiology, Aarhus University Hospital, Denmark and Danish Epilepsy Centre, Dianalund, Denmark

^d Department of Neuroscience and Biomedical Engineering, School of Science, Aalto University, Espoo, Finland

HIGHLIGHTS

- Analysis of initial seizure activity using combined high-density EEG/MEG and novel on-scalp MEG (osMEG).
- Our study demonstrates that osMEG exhibits a unique ability to detect seizure onset zones non-invasively.
- Indicate that osMEG might improve intracranial EEG planning and epilepsy surgery results.

ARTICLE INFO

Article history:

Accepted 21 October 2023

Available online

Keywords:

Epilepsy surgery

Seizure onset zone localization

On-scalp magnetoencephalography

Modeling

Instrumentation

ABSTRACT

Objective: Epilepsy surgery requires localization of the seizure onset zone (SOZ). Today this can only be achieved by intracranial electroencephalography (iEEG). The iEEG electrode placement is guided by findings from non-invasive modalities that cannot themselves detect SOZ-generated initial seizure activity. On scalp magnetoencephalography (osMEG), with sensors placed on the scalp, demonstrates higher sensitivity than conventional MEG (convMEG) and could potentially detect early seizure activity. Here, we modeled EEG, convMEG and osMEG to compare the modalities' ability to localize SOZ activity and to detect epileptic spikes.

Methods: We modeled seizure propagation within ten epileptic networks located in the mesial and lateral temporal lobe; basal, dorsal, central and frontopolar frontal lobe; parietal and occipital lobe as well as insula and cingulum. The networks included brain regions often involved in focal epilepsy. 128-channel osMEG, convMEG, EEG and combined osMEG + EEG and convMEG + EEG were modeled, and the SOZ source estimation accuracy was quantified and compared using Student's t-test.

Results: OsMEG was significantly (p -value < 0.01) better than both convMEG and EEG at detecting the earliest SOZ-generated seizure activity and epileptic spikes, and better at localizing seizure activity from all epileptic networks ($p < 0.01$).

Conclusions: Our modeling results clearly show that osMEG has an unsurpassed potential to detect both epileptic spikes and seizure activity from all simulated anatomical sites.

Significance: No clinically available non-invasive technique can detect SOZ activity from all brain regions. Our study indicates that osMEG has the potential to become an important clinical tool, improving both non-invasive SOZ localization and iEEG electrode placement accuracy.

© 2023 International Federation of Clinical Neurophysiology. Published by Elsevier B.V. This is an open access article under the CC BY license (<http://creativecommons.org/licenses/by/4.0/>).

1. Introduction

On scalp magnetoencephalography (osMEG) is a novel, non-invasive neuroimaging technique that enables MEG sensors to be

placed directly on the scalp instead of in a helmet, as is done in conventional MEG (convMEG). Several types of osMEG sensors have been developed to date (Boto et al., 2018, 2016; Hill et al., 2020; Kanno et al., 2022; Pfeiffer et al., 2020), but only the commercially available optically pumped magnetometers (OPMs) can yet achieve whole-head coverage (Hill et al., 2020; Koshev et al., 2021).

* Corresponding author at: Department of Clinical Neuroscience, Karolinska Institutet, Stockholm, Sweden.

E-mail address: karin.westin@ki.se (K. Westin).

ConvMEG sensors are housed within a one-size-fits-all helmet inside a thermally insulated dewar, which on average results in a 20–40 mm sensor-to-scalp distance (Heiden, 1991; Iivanainen et al., 2017; Riaz et al., 2017). Furthermore, any head movement within this rigid sensor array makes extensive post-recording filtering necessary (Taulu and Simola, 2006). More recently, both experimental and modeling studies have demonstrated that osMEG sensors placed directly to the scalp, with only 3–5 mm separation between the scalp and sensitive volume of the sensor, result in a significantly increased information content compared to convMEG sensors (Iivanainen et al., 2017; Schneiderman, 2014). When mounting osMEG sensors in an individualized cap or a helmet adjustable to head shape, sensor movements will follow head movements, significantly reducing artifacts from head movement relative to the sensors (Boto et al., 2018; Hill et al., 2020). Thus, osMEG enables qualitatively improved, whole-head, high-resolution functional neuroimaging measurements that promise to offer new clinically valuable information during presurgical epilepsy evaluations.

Today, convMEG is routinely used to detect and estimate the localization of interictal epileptiform discharges (IEDs) which occur in between epileptic seizures (Hari et al., 2018; De Tiège et al., 2017, 2012). IED source estimates are used in conjunction with a battery of clinical and other non-invasive neuroimaging evaluations to estimate the localization of the so-called seizure onset zone (SOZ). Thereafter, in some patients invasive intracranial stereo EEG electrodes are implanted to pinpoint the SOZ, based upon the non-invasive evaluation results. Optimally, the sEEG electrodes should be placed *within* the SOZ (Jayakar et al., 2016, 2014). A large number of clinical studies have demonstrated that convMEG IED source estimations *does* increase the likelihood of correct sEEG electrode implantation within the SOZ. These studies have clearly demonstrated that adding convMEG, and especially combined convMEG + EEG significantly increases the probability of post-surgical seizure freedom (Duez et al., 2016; Rampp et al., 2019).

However, IEDs detected by convMEG are not necessarily generated within the SOZ, but may stem from later, propagated activity along a widespread patient-specific epileptic network. Thus, the IED-based convMEG source estimation may not necessarily coincide with the SOZ (Rampp et al., 2019; Duez et al., 2019, 2016). Although ictal convMEG recordings have been performed and offer better accuracy for SOZ localization (Medvedovsky et al., 2012), routine clinical ictal convMEG measurements are impractical for several reasons (Alkawadri et al., 2018). Very long (days) recordings are not possible in the convMEG sensor system as it requires patients to lie or sit relatively still. Furthermore, many seizures are associated with involuntary movements which could result both in large movement artifacts, as well as in a potential risk of injury in case the patient would hit their head against the inside of the fixed convMEG helmet. Since osMEG sensors allow for free head movement (Boto et al., 2021, 2018, 2016), this technology may allow for routine ictal MEG recordings which could increase the probability of accurate sEEG electrode implantation.

Focal epilepsy patients with pharmacoresistant epilepsy and non-lesional structural MRI scans often exhibit highly complex epileptic networks. Hence, while the seizure activity may have its onset in a small cortical region, it often propagates along patient-specific pathways, involving gradually larger cortical areas (Stefan and da Silva, 2013). Consequently, accurate localization of the SOZ requires high sensitivity to the underlying signal to enable the detection and subsequent localization of the weak, initial sources. Today, only intracranial registrations are considered sufficiently sensitive to reliably localize the high-frequency, low-amplitude activity associated with such seizure initiation (Jayakar et al., 2016, 2008; Toth et al., 2019). The improved

proximity that comes with osMEG sensors improves the sensitivity to underlying signals, and hence holds the promise of detecting weaker, earlier signals than convMEG.

In agreement with experimental and modeling studies which show higher signal strength and better spatial accuracy in osMEG compared to convMEG, we have previously demonstrated that osMEG sensors indeed detect more (about twice as many) IEDs than convMEG, and also that osMEG sensors detect IEDs that are too small to be detected by convMEG or EEG (Westin et al., 2020; see also Iivanainen et al., 2017; Riaz et al., 2017; Schneiderman, 2014; Xie et al., 2015).

In this study, we used a modeling approach to further investigate the potential of osMEG, as compared to convMEG and EEG, in detecting and localizing small SOZs of propagating seizure activity. To resemble a clinical presurgical epilepsy evaluation scenario, we simulated epileptic networks originating from ten different anatomical sites. SOZ detection sensitivity and localization accuracy of osMEG was then evaluated and compared to convMEG and EEG. Utilizing a modeling approach allows us to control and validate the exact SOZ localization, which would not be possible in a clinical study. Our study thus entails an exploratory modeling work meant to determine what osMEG is capable of. This approach can help guide future development in the technology itself and may help guiding osMEG recordings on epilepsy patients.

2. Material and method

To resemble a clinical non-invasive neurophysiological presurgical epilepsy evaluation, epileptic networks were simulated with an initial low-amplitude, high-frequency activity with subsequent spatiotemporal evolution. Both sensor and background brain noise were modeled to mimic actual recordings. Ictal osMEG source imaging was modeled and compared to ictal convMEG and EEG source imaging.

2.1. Anatomical model

We used the anatomical model from the sample data set of the MNE-Python software (Gramfort et al., 2013). The model includes an original T1 MPRAGE sequence MRI acquired with a 1.5-Tesla Siemens MRI scanner. A full segmentation of the head and brain was performed using FreeSurfer (Dale et al., 1999; Fischl et al., 1999). A source space with 16,386 sources per hemisphere was constructed.

2.2. Forward model

An identical three-compartment (skin, skull, and brain) conductor model was used for osMEG, convMEG, and EEG. The boundaries between the compartments were based on FreeSurfer segmentation and the linear collocation boundary-element modeling approach was used in MNE-Python for magnetic field and electric potential calculations (Gramfort et al., 2013).

2.3. Sensor arrays

OsMEG, convMEG and EEG were all modeled separately. In addition, combined sensor arrays with osMEG + EEG, and convMEG + EEG were also modeled.

2.3.1. OsMEG

The sensors were modeled as optically pumped magnetometers (OPM) sensor cubes with side length 10 mm. The sensor output was computed by integration over a sensing volume of $3 \times 3 \times 3 \text{ mm}^3$ 5 mm from the outer wall. Previous experimental

and modeling studies reported noise levels of 6–15 fT/Hz^(1/2) in osMEG sensors. To make sure we do not underestimate the influence of noise, we opted for a more conservative noise level of 30 fT/Hz^(1/2), which is more than twice what has been measured with osMEG (Boto et al., 2021; Osborne et al., 2018). An array of 128 sensors was modeled and placed with 1 cm inter-sensor distance over the scalp. The sensors had a 1 mm standoff in accordance with other osMEG simulation studies.

2.3.2. ConvMEG

A conventional MEG 306-channel VectorView system (MEGIN OY, Helsinki, Finland) sensor array was modeled using MNE Python. The magnetic fluxes that thread the SQUID detection coil constitute the sensor output. The flux can be determined as the integral of the magnetic field normal to the coil plane. Here, the sensor output was thus determined by integration of the SQUID pickup coil using 4 integration points. Noise levels were set to 5 fT/cm/Hz^(1/2) and 5 fT/Hz^(1/2) for gradiometers and magnetometers, respectively.

2.3.3. EEG

60 EEG channels were simulated and placed according to the 10–10 montage. For each electrode, the electric potential at the center of the electrode was calculated as the sensor output. The EEG noise sensor noise levels were set to 4 microV/Hz^{1/2} (Ryynänen et al., 2004).

2.3.4. Combined sensor arrays

A combined sensor array with both a 128 osMEG and a 10–10 EEG montage was created by placing the osMEG sensors between the EEG electrodes (see Fig. 1 for a schematic overview of a possible combined osMEG-EEG sensor array).

2.4. Activity simulations

2.4.1. Epileptic networks

Ten epileptic networks were modeled, with the SOZ located in the frontal lobe, insula, temporal lobe, parietal lobe, occipital lobe, and the cingulum. To cover anatomical sites often engaged in focal epilepsy, four of these SOZs were placed in the frontal lobe (polar frontal region, basal frontal lobe, lateral frontal lobe and the central region), two SOZs were placed in the temporal lobe (mesial temporal lobe and lateral temporal lobe), and one SOZ was placed in the insula (Engel, 2001; Tatum, 2012; Kellinghaus and Lüders, 2004; Blume et al., 2001). To simulate migrating ictal activity, 16 adjacent cortical patches were chosen. These were defined as circular patches on the inflated FreeSurfer cortical surface, with gradually growing radii. Starting with a SOZ radius of 4 mm, the radius increased by 1 mm for each subsequent patch. Each patch was active for three seconds. To resemble human seizure activity with spatiotemporal evolution, the SOZ generated high frequency (100 Hz) activity. To simulate ictal spatiotemporal evolution, the next patch generated high frequency activity (50 Hz), followed by a patch generating 35 Hz activity (Olmi et al., 2019; Proix et al., 2018). Remaining patches generated rhythmic spike and wave activity, simulated using the Wendling model, a neural mass model designed to generate ictal activity (Wendling et al., 2016, 2002). For each cortical patch, dipole density was set to $q = 0.77$ nAm/mm² (Murakami and Okada, 2015). For the anatomical distributions of the simulated epileptic networks as well as a summary of the size of the activated cortex at the different simulation time points, see Fig. 2.

2.4.2. Epileptic spike simulation

In addition to epileptic networks, epileptic spikes were simulated to originate from each of the ten SOZs described in Sec-

tion 2.4.1. The Wendling model was then used to simulate isolated epileptic spikes from gradually growing cortical regions. The initial radius was set to 4 mm, and thereafter grew by 1 mm until it reached 15 mm. These epileptic spikes did not propagate but were only set to include an increasingly large region of the cortex. The cortical regions sizes that gave rise to identifiable epileptic spikes in osMEG, convMEG and EEG respectively were statistically compared using Student's t-test.

2.4.3. Brain noise

The background brain noise model for both osMEG, convMEG and EEG was based upon a MEG + EEG resting state recording from the MNE Python sample participant. A minimum norm estimate distributed source estimate solution was then computed for 500 seconds resting data. The solution was computed using MNE Python. The weight of source variance of dipoles parallel to the cortical surface, and the depth prior weight of the forward solution (parameters “loose” and “depth” in the MNE function *make_inverse_solution*), were set to 0.2 and 0.8, respectively. The regularization parameter was set to $1/\text{SNR}^2$ (signal to noise ratio, SNR) with SNR = 3. Pooling was performed by taking the norm of the free source orientations (Gramfort et al., 2013). The source estimate was computed for a source space model with 16,386 sources per hemisphere. Hereafter, the distributed solution was added to the anatomical model used for ictal activity simulation.

2.5. Sensor data generation

Epileptic networks, epileptic spikes, and brain noise were added to the source space of the anatomical model (one for each epileptic network). Using the MNE Python function *simulate_raw* both osMEG, convMEG, EEG and combined convMEG + EEG as well as combined osMEG + EEG sensor data were simulated.

2.6. Clinical evaluation of raw sensor data

Similar to routine clinical MEG + EEG epilepsy evaluations, the raw sensor data sets (one osMEG, one convMEG, one EEG, and one convMEG + EEG data set for each epileptic network) underwent visual inspection by an experienced clinician (author KW). Although several algorithms have been developed for experimental seizure activity detection, none of these are routinely used within clinical settings. Instead, clinical guidelines recommend visual identification of initial seizure activity characterized by high-frequency, low-amplitude activity performed by experienced epileptologists (Blume et al., 2001; Kane et al., 2017). However, in addition to visual inspection, we also performed time–frequency analysis of the raw data to identify any sudden onset of time–frequency changes associated with seizure onset. After identification of seizure activity, using both visual inspection and time–frequency analyses, source imaging was performed for the first second (one second epoch) of the detected seizure activity. Equivalent current dipoles (ECDs) were computed for both the osMEG, convMEG and EEG data, and the combined convMEG + EEG as well as combined osMEG + EEG data (Sarvas, 1987). MNE Python in-built function *fit_dipole()* was used with a default parameter setting for ECD calculation. The noise covariance was determined using a 0.5 second data epoch immediately preceding onset of seizure activity. The distance between the osMEG, convMEG, EEG, convMEG + EEG, and osMEG + EEG ECDs and the center of the SOZ was computed for each epileptic network. Student's t-test was utilized to compute any statistically significant difference between the osMEG ECD-SOZ center distance, and the convMEG, EEG and convMEG + EEG as well as osMEG + EEG ECD-SOZ center distance. In case the SOZ high frequency activity was not visible in the convMEG and/or EEG raw sensor data, the

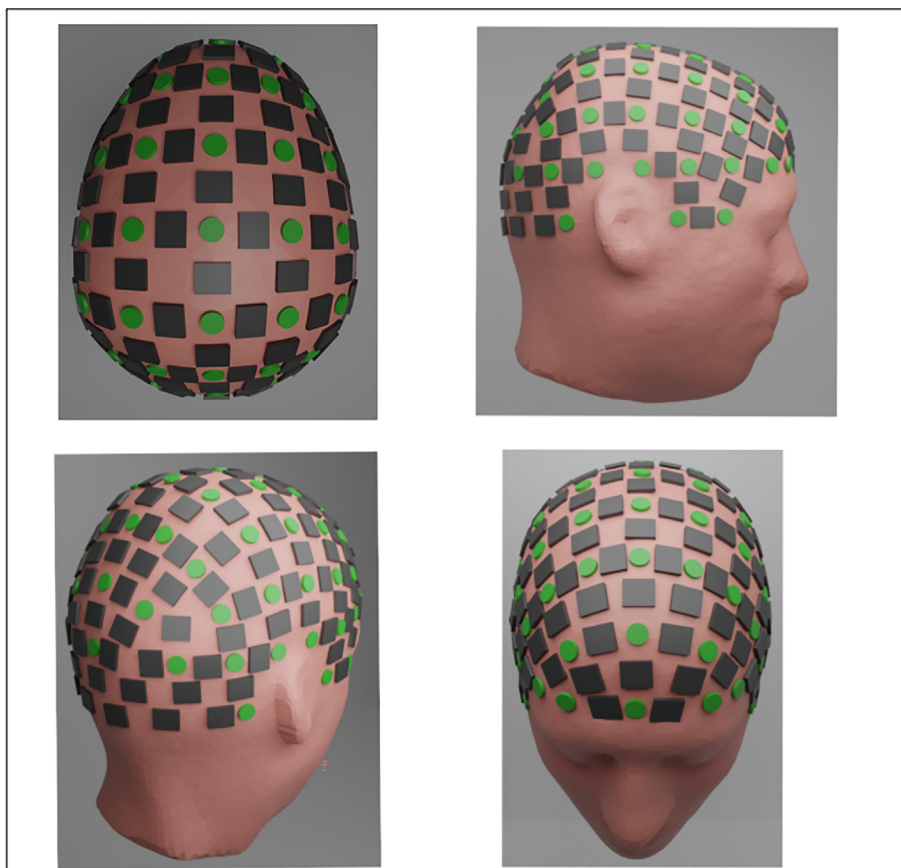


Fig. 1. Proposed combined on scalp magnetoencephalography (MEG) – electroencephalography (EEG) sensor layout. Black: Sensor layout of 128 on scalp magnetoencephalography (MEG) sensors Green: Sensor layout of 65 electroencephalography EEG electrodes in a 10–10 montage.

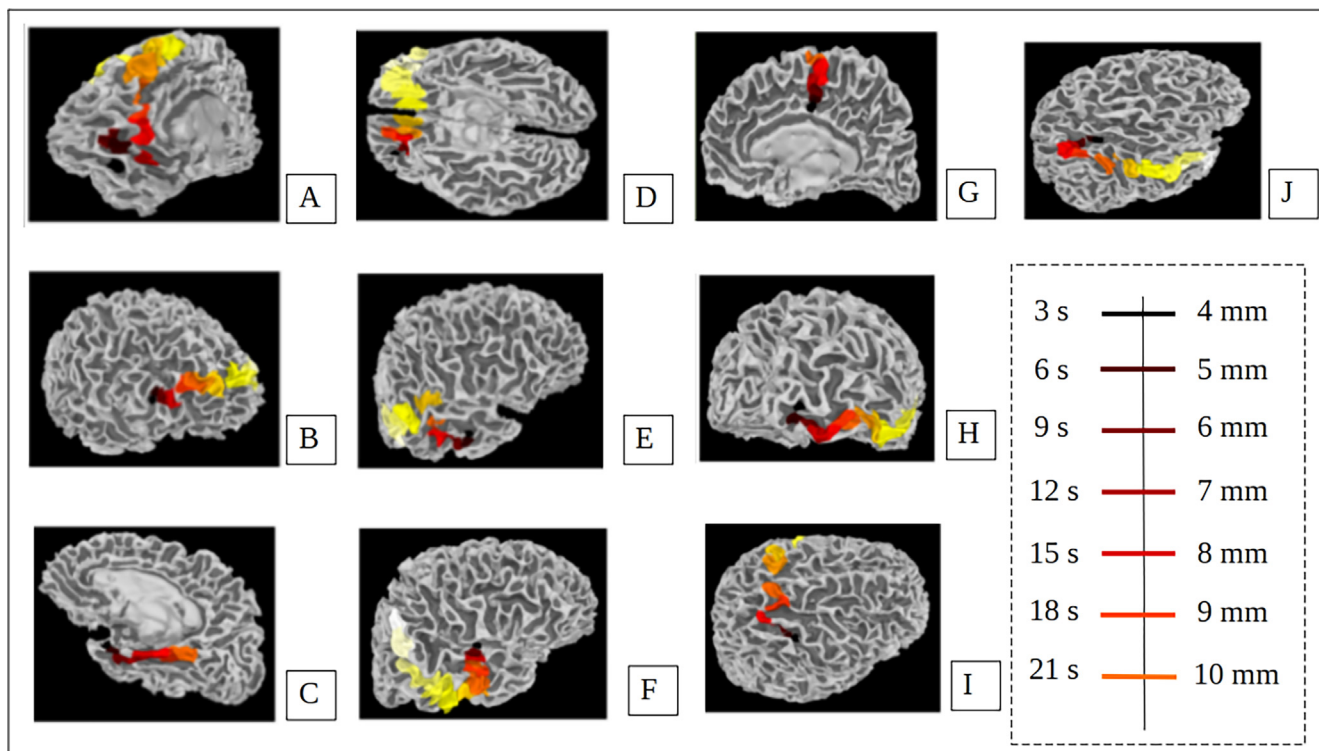


Fig. 2. Anatomical distribution of epileptic networks. Anatomical distribution of epileptic networks with seizure onset zone (SOZ) in black and propagating seizure activity in red, orange, and yellow. (A: frontopolar, B: basal frontal lobe; C: lateral frontal lobe; D: lateral temporal lobe; E: mesial temporal lobe; F: insula, G: central region; H: cingulum; I: parietal lobe; J: occipital lobe). Sub-figure on bottom right indicate the size of the epileptic network at times 3, 6, 9, ..., 21 seconds.

distance between the convMEG + EEG ECD and the center of the region generating the first visible ictal activity was computed in order to evaluate the accuracy of the simulated recording. See Fig. 3 for an illustration of how the source localization accuracy was determined. See Fig. 4 for selected raw sensor space data traces of seizure activity from osMEG data; Fig. 5 for selected raw sensor space data traces of seizure activity from convMEG data and Fig. 6 for selected raw sensor space data traces of seizure activity from EEG data.

3. Results

3.1. Seizure activity detection in raw sensor space data

3.1.1. OsMEG

For all anatomical sites except the mesial temporal lobe, low amplitude very high frequency SOZ (radius = 4 mm, area = 0.5 cm²) activity was visible in the osMEG raw sensor data. Mesial temporal lobe seizure activity was visible in the osMEG sensor space data once the seizure activity had propagated to a cortical source with a radius of 5 mm (area = 0.79 cm²). The results from visual inspection were verified by time frequency analysis of the raw sensor data. For all sites except the mesial temporal lobe, an increase of high-frequency (100 Hz) activity was seen at time 3 seconds (onset of earliest seizure activity). For mesial temporal lobe, 50 Hz activity was identified at time 6 seconds (see Fig. 4 for both raw initial ictal

activity from osMEG sensor space data and the corresponding spectrogram from selected epileptic networks).

3.1.2. ConvMEG

The earliest visually identifiable seizure activity in convMEG raw sensor data was propagated seizure activity originating from a cortical source with a radius of 8 mm (area = 2.01 cm²). This source size was thus 4 times larger than the source that could generate visually identifiable seizure activity in osMEG raw sensor data (see section 3.1.1 above). The time–frequency analysis showed that the initial seizure activity was characterized by rhythmic 8–12 Hz activity. See Fig. 5 for both raw convMEG ictal sensor space data and the corresponding spectrogram for selected epileptic networks.

3.1.3. EEG

Similar to convMEG, the earliest visually identifiable seizure activity in EEG raw sensor data was propagated seizure activity originating from a cortical source of area 2.01 cm² (radius = 8 mm). See Fig. 6 for both raw EEG ictal sensor space data, and for the corresponding spectrogram for selected epileptic networks.

3.1.4. Combined sensor arrays

Combining osMEG + EEG and convMEG + EEG sensor arrays did not further improve seizure activity detection in the raw sensor data. The time–frequency analysis revealed that the first identifiable seizure activity was characterized by rhythmic 8–12 Hz activity.

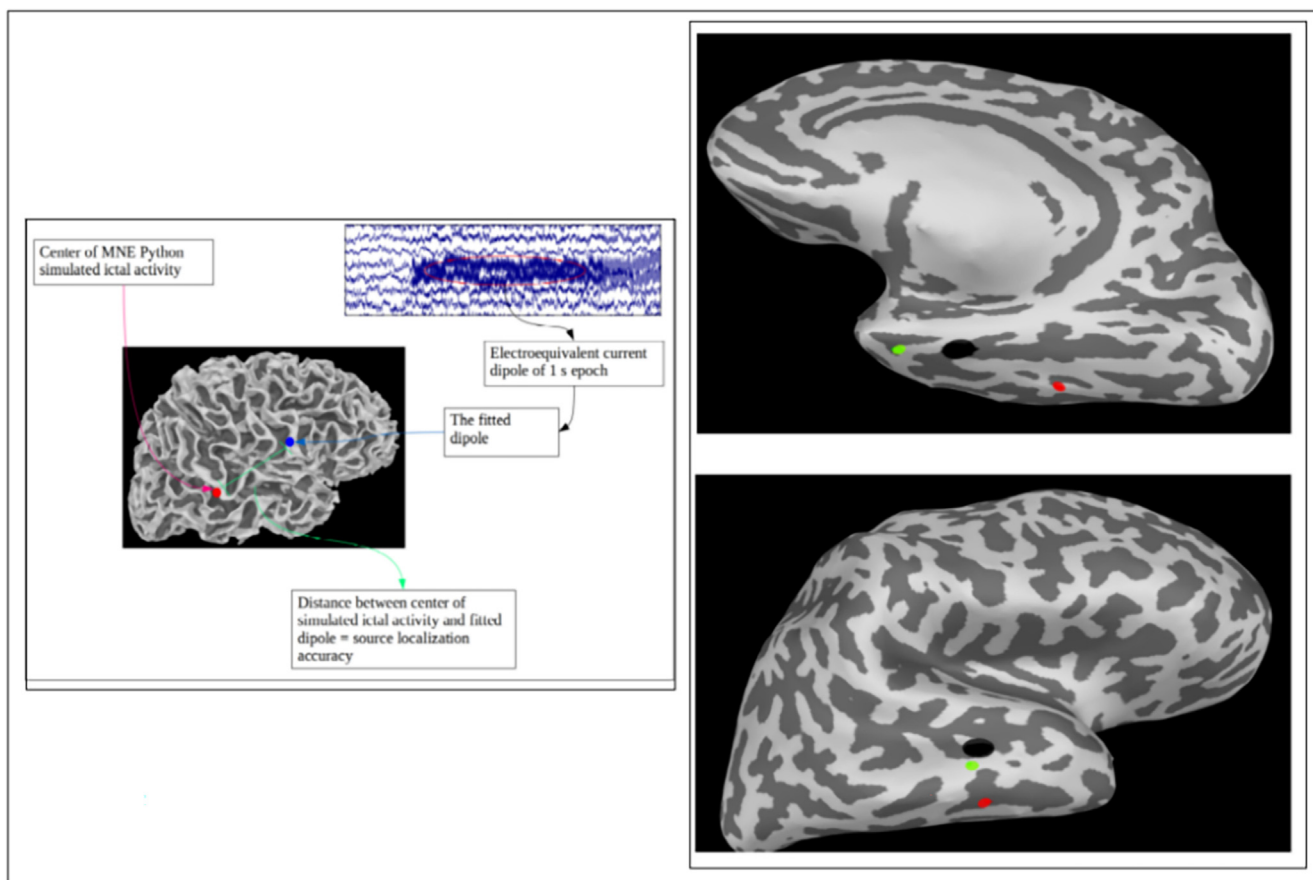


Fig. 3. Source localization metric and source localization accuracy of the temporal lobe. Left: Illustration of the source localization accuracy metric utilized. Right: Source localization of initial ictal activity from on scalp MEG (osMEG) (green) and combined conventional MEG and EEG (convMEG plus EEG) (red). Black: Seizure onset zone. Top: Mesial temporal lobe; bottom: lateral temporal lobe.

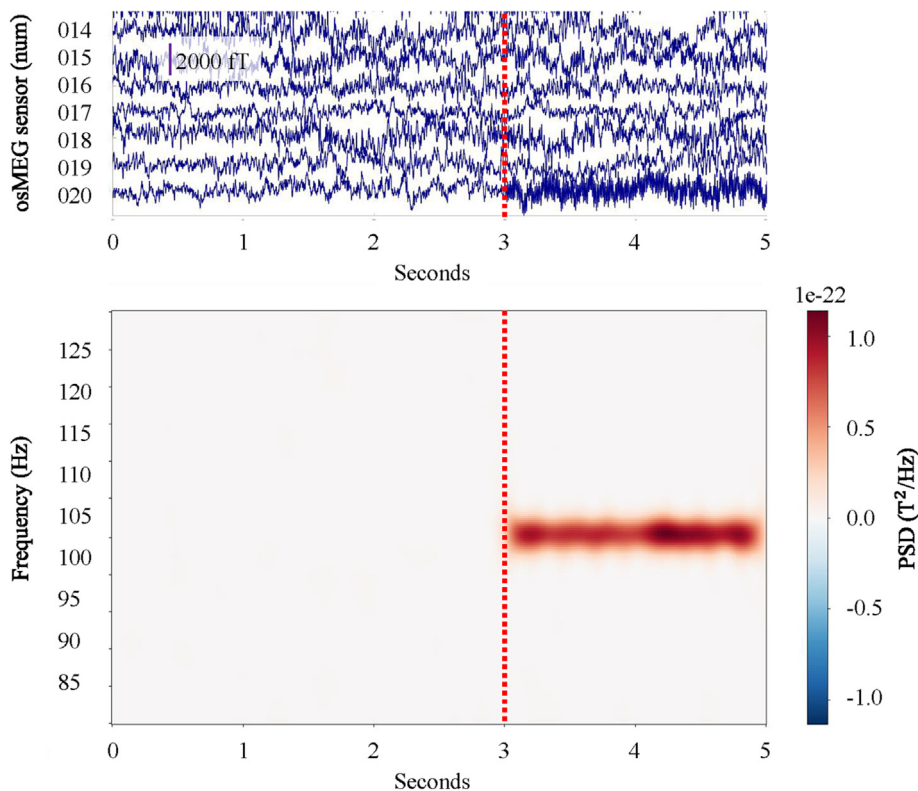


Fig. 4. On scalp MEG (OsMEG) raw sensor space data and spectrograms from the basal frontal lobe. Top: Raw on scalp MEG (osMEG) sensor data of initial ictal activity from the basal frontal lobe at starting at time 3 seconds (onset marked by dashed pink line). The sensor data was filtered 1–130 Hz using a one-pass, zero-phase non-casual time-domain finite impulse filter. Bottom: Spectrogram of the data trace on top demonstrating upregulation of 100 Hz activity at time 3 seconds. Raw sensor data and spectrograms for three additional epileptic networks can be found in the Supplementary Material.

3.2. Seizure onset zone source estimations based on earliest visually identifiable seizure activity

ECDs of the earliest visually identifiable seizure activity in both osMEG (low amplitude, very high frequency SOZ activity for all sites but mesial temporal lobe) and in convMEG + EEG (propagated seizure activity for all sites) were computed, and the distances between these ECDs and the ten SOZ centers calculated. The resulting average ECD-SOZ center distances were 4.7 mm (range: 2.2–9.6 mm) for osMEG and 20.15 mm (range: 14.2–29.8 mm) for convMEG + EEG, respectively. Consequently, the mean osMEG ECD-SOZ center distance was 4.3 times smaller (i.e., the source localization accuracy was 4.3 times better) than the mean convMEG + EEG ECD-SOZ center distance. The osMEG ECD-SOZ center distances were statistically smaller than the convMEG + EEG ECD-SOZ center distances (p -value < 0.01). See also Table 1 and Fig. 3 for osMEG and convMEG + EEG source localization accuracy for two epileptic networks.

The mean convMEG ECD-SOZ distance was 20.37 mm (range: 15.9–29.4 mm). The mean EEG-ECD SOZ distance was 21.55 mm (range: 16.0–29.1 mm). The osMEG ECD-SOZ center distance was significantly smaller than both the convMEG and the EEG ECD-SOZ distance. See Table 1 for an overview. See also Fig. 3 for localization of SOZs as well as osMEG and convMEG plus EEG ECDs for two of the epileptic networks.

In addition, we also computed combined convMEG + EEG source localization accuracy of the earliest seen seizure activity in these modalities. In all epileptic networks, this earliest visually identifiable activity originated from propagated seizure activity. The mean localization accuracy for this propagated activity was 4.49 mm (range: 1.90–6.60 mm). See Table 1 for details.

3.3. Epileptic spike detection and source estimations

Epileptic spikes were first seen in the osMEG data. For all sites but the frontopolar region and the insula, epileptic spikes originating from a cortical patch of size 0.5 cm² were visible in raw sensor data. Epileptic spikes from the frontopolar region and the insula were visible when originating from a cortical region of size 0.78 cm². Mean cortical area size for visible osMEG epileptic spikes was 0.56 cm². The corresponding mean size for convMEG was 1.91 cm² and 1.87 cm² for EEG. OsMEG cortical area sizes were hence significantly smaller than those of convMEG and EEG (p -value < 0.01). Epileptic spikes and initial ictal activity (section 3.2) were thus seen at approximately the same time. There was no significant difference between the modalities' source localization accuracy. See Table 2 for an overview and Fig. 7 for raw data traces with epileptic spikes in osMEG, convMEG, and EEG.

4. Discussion

Unlike convMEG systems, the osMEG sensor system places sensors directly on the scalp and thereby significantly improves the proximity to the cortex which enhances the capability to detect and localize small cortical sources by approximately a factor of 4. OsMEG furthermore allows for free head movement during recordings and thus allows for longer recordings than convMEG, thereby potentially enabling routine ictal MEG recordings. The results from this study suggest that osMEG offers a unique potential to significantly improve non-invasive detection as well as source estimation accuracy for initial SOZ activity. OsMEG thereby holds the promise

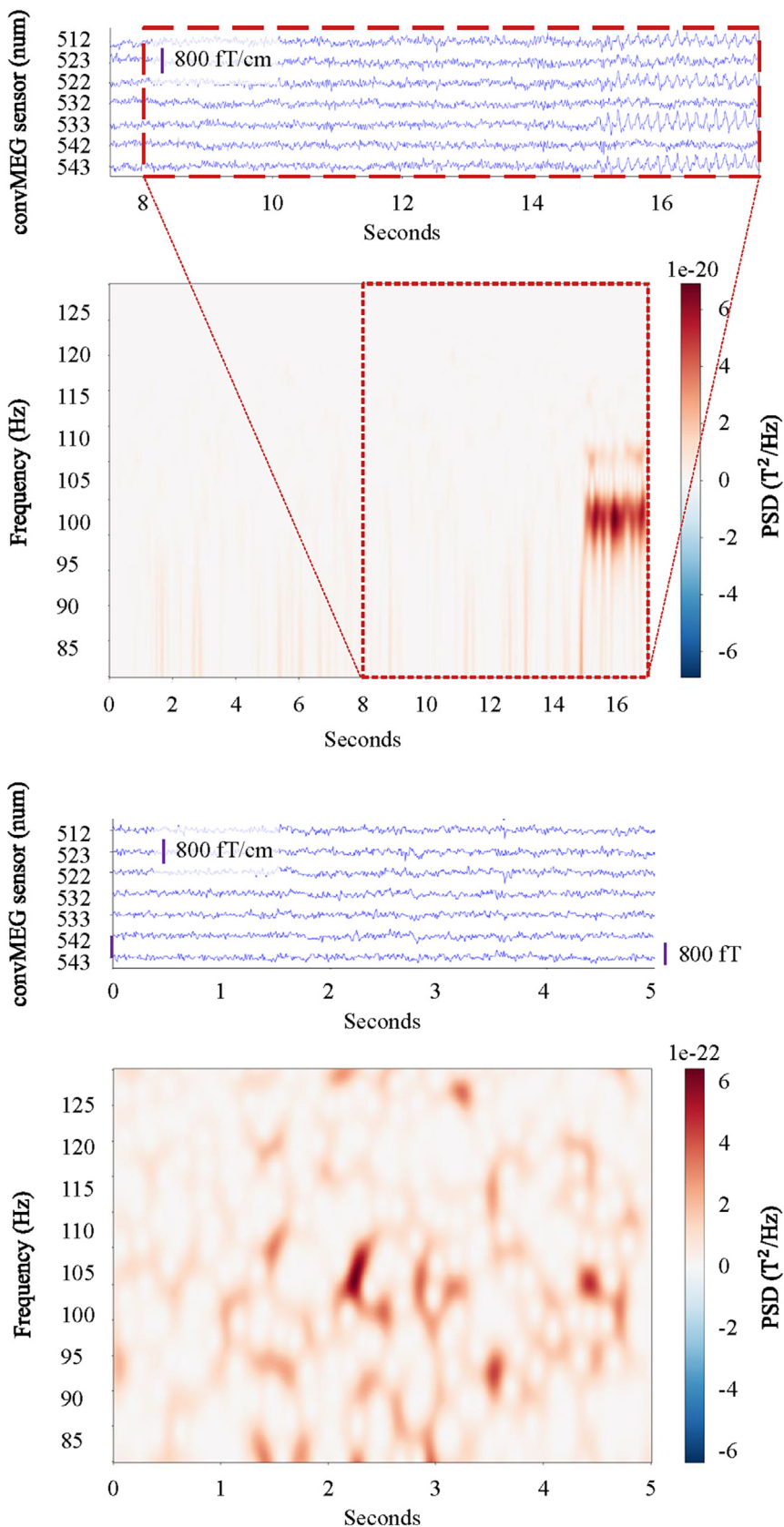


Fig. 5. Conventional MEG (ConvMEG) raw sensor space data and spectrograms from the cingulum. Top: First visible ictal activity from the cingulum seen in conventional MEG (convMEG) at time 15 seconds with corresponding spectrogram demonstrating upregulation of 8–12 Hz activity at time 15 seconds (onset marked by dashed black line). The sensor data was filtered 1–130 Hz using a one-pass, zero-phase non-casual time-domain finite impulse filter. Bottom: Initial 5 seconds of the same sensors as presented above with corresponding spectrogram without any upregulation of high frequency activity as seen in the on scalp MEG (osMEG data) (see Fig. 4). Raw sensor data and spectrogram for one additional epileptic network can be found in the Supplementary Material.

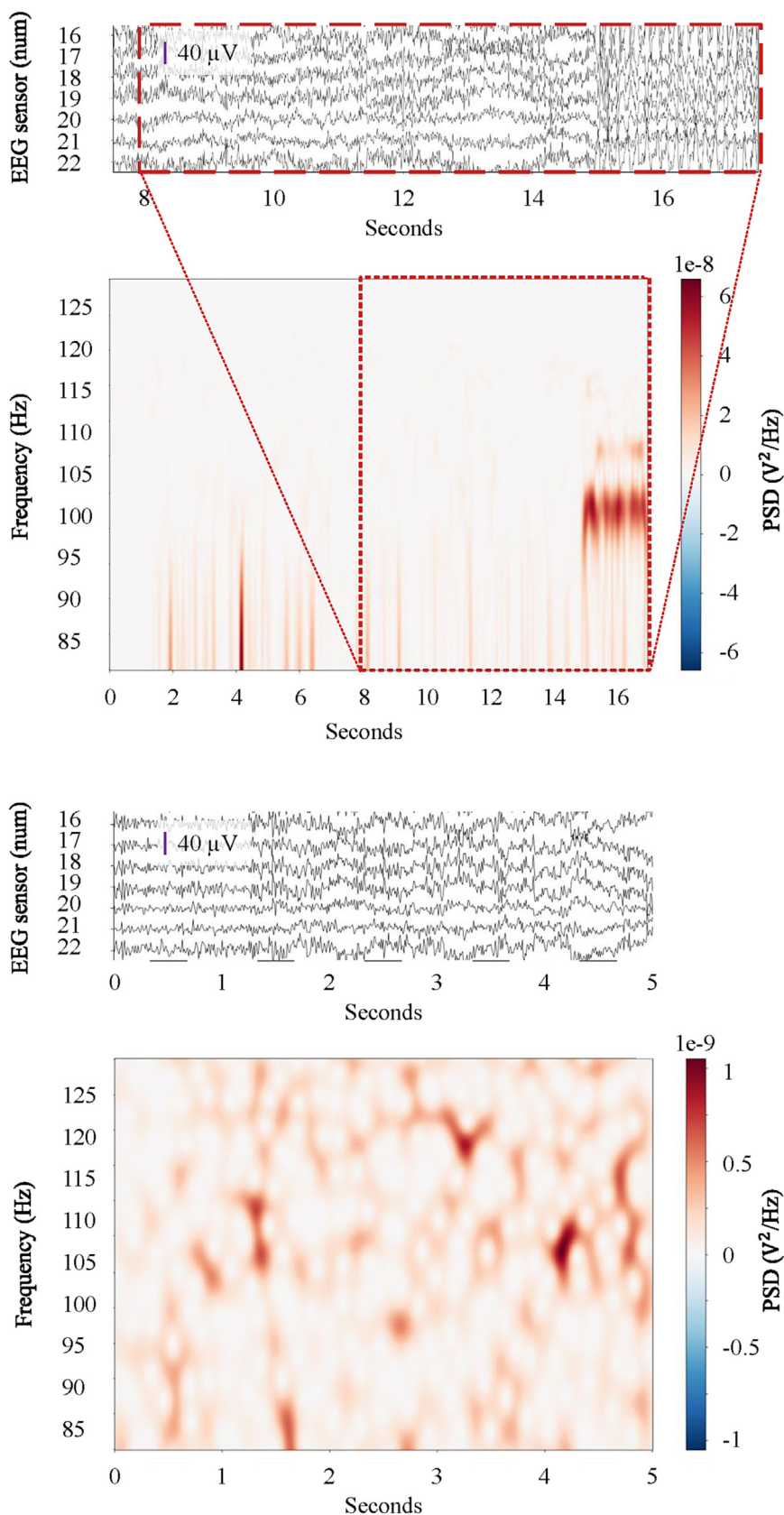


Fig. 6. EEG raw sensor space data and spectrograms from the lateral frontal lobe. Top: First visible ictal activity from the lateral frontal lobe seen in EEG at time 15 seconds with corresponding spectrogram demonstrating upregulation of 8–12 Hz activity at time 15 seconds (onset marked by dashed blue line). The sensor data was filtered 1–130 Hz using a one-pass, zero-phase non-casual time-domain finite impulse filter. Bottom: Initial 5 seconds of the same sensors as presented above with corresponding spectrogram without any upregulation of high frequency activity as seen in the on scalp MEG (osMEG data) (see Fig. 4). Raw sensor data and spectrogram for one additional epileptic network can be found in the Supplementary Material. For EEG electrode placements on scalp, please see Supplementary Fig. 8. The simulated electrodes record the electric potential at specific scalp coordinates, and not the difference between scalp positions as in experimental settings.

Table 1

On scalp MEG (osMEG), conventional MEG (convMEG), EEG (EEG) and combined convMEG + EEG seizure activity detection and Equivalent Current Dipole (ECD) – seizure onset zone (SOZ) center distances.

Anatomical site	Type of earliest seen seizure activity: SOZ or propagated		SOZ source localization accuracy (mm)			Accuracy in localizing earliest seen seizure activity (SOZ or propagated) (mm)	
	osMEG	convMEG and EEG	osMEG	convMEG + EEG	convMEG (EEG)	osMEG	convMEG + EEG
Frontopolar	SOZ	Propagated	6.1	14.9	15.9 (16.6)	6.1 (S ⁺)	5.5 (P)
Basal frontal lobe	SOZ	Propagated	3.1	14.2	14.8 (16.0)	3.1 (S)	6.6 (P)
Lateral frontal lobe	SOZ	Propagated	2.4	16.4	16.2 (18.1)	2.4 (S)	2.8 (P)
Lateral temporal lobe	SOZ	Propagated	9.6	17.0	17.5 (17.3)	9.6 (S)	3.0 (P)
Mesial temporal lobe	Propagated	Propagated	5.1	26.5	26.0 (26.4)	2.4 (P ⁺⁺)	6.7 (P)
Insula	SOZ	Propagated	6.0	15.6	15.9 (17.9)	6.0 (S)	1.9 (P)
Central region	SOZ	Propagated	5.6	29.8	29.4 (29.1)	5.6 (S)	5.7 (P)
Cingulum	SOZ	Propagated	3.4	19.5	21.3 (24.8)	3.4 (S)	4.1 (P)
Parietal lobe	SOZ	Propagated	3.5	23.6	23.6 (25.7)	3.5 (S)	3.7 (P)
Occipital lobe	SOZ	Propagated	2.2	24.0	23.1 (23.4)	2.2 (S)	4.9 (P)
Mean			4.7^{*,***}	20.15	20.37 (21.54)	4.43	4.49

S⁺ First seen seizure activity from SOZ.

P⁺⁺ First seen seizure activity from propagated seizure activity.

Abbreviations: convMEG: conventional magnetoencephalography; EEG: electroencephalography; osMEG: on scalp magnetoencephalography; SOZ: seizure onset zone.

* OsMEG distance between earliest seen activity significantly smaller than ConvMEG/EEG distance between earliest seen activity.

** OsMEG distance between earliest seen activity significantly smaller than ConvMEG distance between earliest seen activity.

*** OsMEG distance between earliest seen activity significantly smaller than EEG distance between earliest seen activity.

Table 2

Comparison of the cortical region size that give rise to identifiable epileptic spikes in conventional MEG, on scalp MEG, and EEG data for all anatomical sites.

Anatomical site	OsMEG (cm ²)	OsMEG source localization accuracy (mm)	ConvMEG (cm ²)	ConvMEG source localization accuracy (mm)	EEG (cm ²)	EEG source localization accuracy (mm)
Frontopolar	0.78	5.6	2.01	5.1	1.54	5.5
Basal frontal lobe	0.5	6.0	2.02	7.0	2.01	6.9
Lateral frontal lobe	0.5	3.5	2.01	3.1	2.01	4.1
Lateral temporal lobe	0.5	5.3	2.01	5.6	2.01	4.6
Mesial temporal lobe	0.5	6.2	1.54	6.1	1.54	6.0
Insula	0.78	6.1	2.02	5.9	2.01	6.3
Central region	0.5	3.4	2.01	3.2	2.01	3.5
Cingulum	0.5	5.5	2.02	5.2	1.54	5.3
Parietal lobe	0.5	2.7	2.01	2.8	2.01	2.7
Occipital lobe	0.5	3.1	2.01	3.5	2.01	2.2
Mean	0.56^{*,**}	4.74	1.91	4.75	1.869	4.71

Abbreviations: convMEG: conventional magnetoencephalography; EEG: electroencephalography; IED: interictal epileptiform discharges; osMEG: on scalp magnetoencephalography.

* Cortical area generating IEDs visible in osMEG raw data significantly smaller than cortical area generating IEDs visible in convMEG.

** Cortical area generating IEDs visible in osMEG raw data significantly smaller than cortical area generating IEDs visible in EEG.

to significantly improve the guidance of sEEG electrode positioning, the guidance of the surgeon and thereby epilepsy surgery outcome.

Epilepsy surgery is performed to remove the seizure onset zone from where seizure activity initiates. Presurgical epilepsy evaluations aim to pinpoint this region by detecting and localizing SOZ-generated initial low amplitude, high frequency activity. This localization is today routinely guided by invasive sEEG measurements (Toth et al., 2019). However, although the ictal activity may be initiated within a small SOZ, pharmacoresistant focal epileptic seizure often propagate along patient-specific pathways within complex epileptic networks (Proix et al., 2018; Stefan and da Silva, 2013). Thus, accurately localizing the SOZ so that it can be targeted by sEEG electrodes can be very difficult, since sEEG electrodes are placed within a limited area of the brain, the choice of which is based on non-invasive neuroimaging investigations that themselves cannot detect the initial SOZ seizure activity (Duez et al., 2019; Jayakar et al., 2016, 2008). Thus, these neuroimaging modalities, including EEG and convMEG, only provide indirect and incomplete evidence of the brain regions that most likely contain the SOZ. Incorrect sEEG electrode positioning due to insufficient or inaccurate non-invasive evaluations do not only result in poor epilepsy surgery results, but also in epilepsy patients

undergoing inconclusive intracranial registrations with potential severe adverse effects (Kwan et al., 2012). Conversely, an accurate and reliable non-invasive SOZ source estimation would significantly improve sEEG electrode area-selection placement accuracy and, in extension, improve epilepsy surgery results.

The osMEG sensor system’s proximity to the cortex allows for a significantly increased sensitivity. In agreement with the expected benefits from this improved proximity, our results show that osMEG may precisely localize even a very small (0.5 cm²) SOZ region at most sites across the cortex. In contrast, combined convMEG + EEG could not detect SOZ activity from any sources of such size (see Fig. 2A and B), requiring cortical regions of 2.5 times that area for detection. Our results therefore suggest that the placement of sEEG implantation would be significantly improved by being guided by osMEG rather than convMEG and/or EEG alone. Furthermore, osMEG allows for free head movement during recordings. This allows for longer recordings than with convMEG, thereby potentially enabling routine ictal MEG recordings, which in turn would enable a more direct localization of the SOZ as compared to interictal recordings that are typically done with convMEG.

The results from this study suggest that osMEG offers a unique potential to significantly improve non-invasive detection as well as

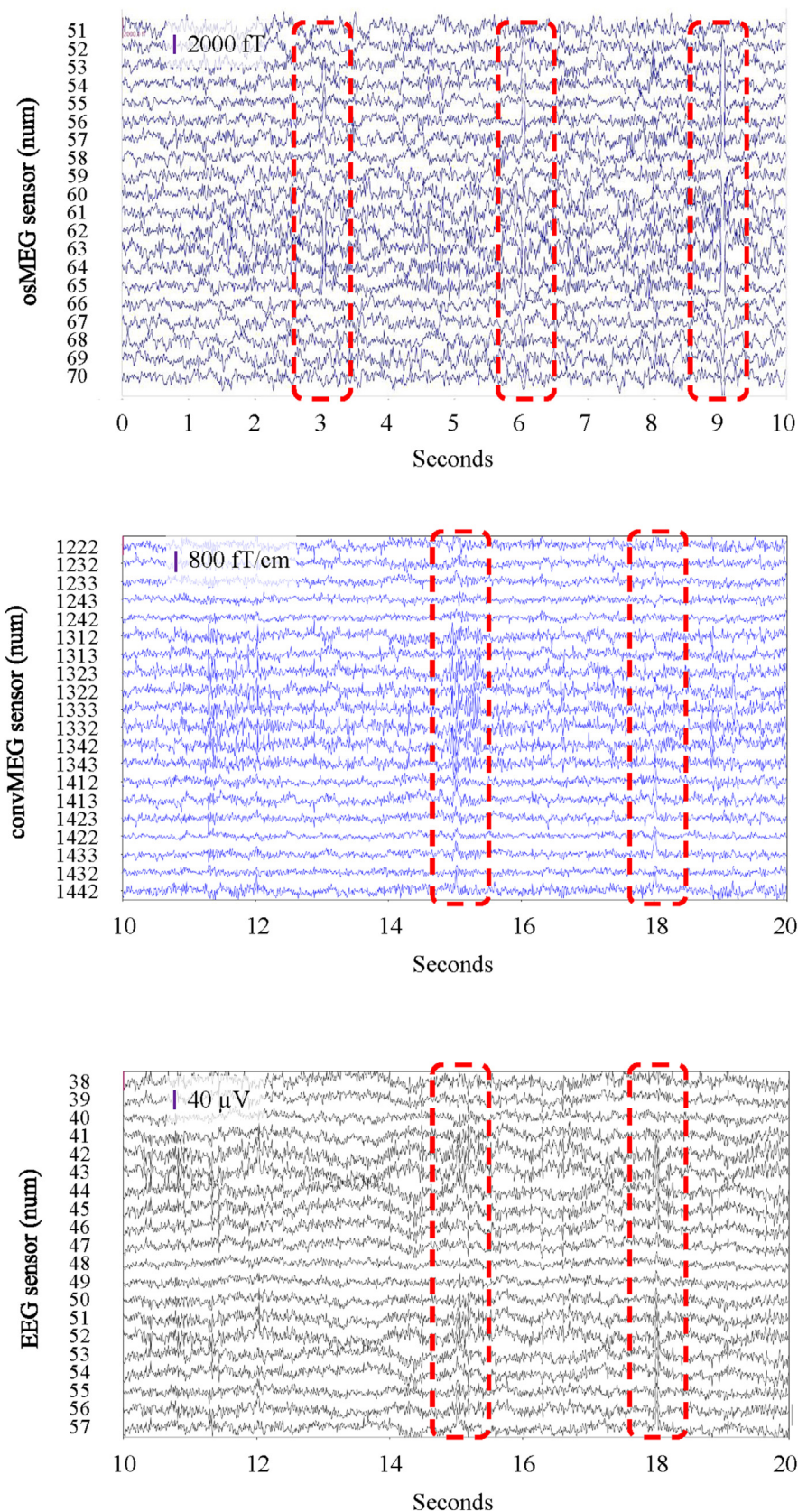


Fig. 7. Epileptic spike visibility in on scalp MEG (osMEG), conventional MEG (convMEG) and EEG from the parietal lobe. Top: Epileptic spikes seen in on scalp MEG (osMEG) at time 3 seconds (area: 0.5 cm²). Middle: Epileptic spike in conventional MEG (convMEG) seen at time 15 seconds (area: 2.02 cm²). Bottom: Epileptic spikes in EEG seen at time 15 seconds (area: 2.02 cm²). The sensor data was filtered 1–40 Hz using a one-pass, zero-phase non-casual time-domain finite impulse filter. Raw sensor data from osMEG, convMEG and EEG from one additional epileptic network can be found in the Supplementary Material. For EEG electrode placements on scalp, please see Supplementary Fig. 8. The simulated electrodes record the electric potential at specific scalp coordinates, and not the difference between scalp positions as in experimental settings.

source estimation accuracy for initial SOZ activity. Thus, osMEG holds the promise to significantly improve sEEG electrode positioning, and thereby epilepsy surgery outcome. One could argue that, in all fairness, the difference in SOZ localization ability stems from the increased signal strength in osMEG compared to convMEG + EEG. While we demonstrated that osMEG could detect sources four times smaller than the sources detected by convMEG + EEG, there were no significant difference in source estimation accuracy between the modalities when comparing osMEG and convMEG + EEG ECDs of visually identifiable epileptic activity (e.g., from sources 2.1 cm² and more). Importantly however, the lower sensitivity of convMEG and EEG utilized in clinical epilepsy evaluations render these techniques less likely to detect *initial seizure activity originating from small cortical sources* such as the SOZ, and more likely to localize the activity somewhere along a propagated network of increasing size. The improved signal strength in osMEG recordings may thus enable routine clinical non-invasive SOZ detection and an improved SOZ localization (see Fig. 2A and B). This critical improvement can potentially move MEG from being a useful neuroimaging tool to becoming instrumental in SOZ localization and sEEG planning.

To date, there are still only a small number of experimental osMEG studies. There is therefore limited knowledge of osMEG sensor and source space data, including osMEG brain noise characteristics. Since several studies have demonstrated an increased osMEG signal strength compared to convMEG, it can be assumed that the brain noise amplitude is also higher than that of convMEG. To achieve realistic brain noise for all analyzed modalities, a real convMEG + EEG recording was utilized to create realistic sensor space background noise activity. To further ensure that the osMEG modality was not favored in the simulation, sensor noise of the osMEG sensors were set conservatively to 30 fT/Hz^(1/2), compared to the levels of 6–15 fT/Hz^(1/2) typically seen in real recordings (Boto et al., 2021; Iivanainen et al., 2017). Furthermore, in order to verify that the simulations used to produce these present results were accurate, we compared the simulated convMEG + EEG performance to experimental results. Such studies have demonstrated that convMEG + EEG ECDs are placed about 5–13 mm from the estimated source (Komssi et al., 2004). Correspondingly, when determining the convMEG + EEG ECD of the first visible ictal activity, and its distance to the cortical region eliciting corresponding visible ictal activity, we found that the convMEG + EEG ECDs were about 6.4 mm from the source, which is then in agreement with experimental studies. Furthermore, in our simulation, we found that epileptic activity was visible in the convMEG + EEG data from activation areas of ~2 cm² (see Table 2). In agreement with these results, co-registrations of convMEG and intracranial EEG during real recordings have concluded that activation of 1–3 cm² cortex is required for convMEG to detect epileptic activity (Oishi et al., 2002). These results are also in agreement with in vivo electrophysiological measurements which have demonstrated that the current dipole density of human neocortical slices is approximately 1–2 nAm/mm² (Murakami and Okada, 2015). Consequently, Murakami and Okada concluded that epileptic spikes visible in convMEG + EEG arise from a minimum of 1.37–2.75 cm² activated cortex (Murakami and Okada, 2015). These conclusions are thus in accordance with the modeling results presented here (see Table 2).

We further found that epileptic spike detection was similar for both convMEG and EEG. Several studies have shown that the different sensitivity profiles of convMEG and EEG reported in the literature depends on depth and orientation (Hunold et al., 2016). Although some studies have demonstrated that high-density EEG detects a greater number of spikes than do convMEG (Plummer et al., 2019), several studies have demonstrated that convMEG detects more epileptic spikes than EEG (Iwasaki et al., 2005; Park et al., 2002, 2004). It is likely that the epileptic networks simulated

here do not exhibit the same depth and orientation profiles as do real epileptic sources, affecting EEG plus convMEG visibility.

Although the main focus of this manuscript is on the potential of osMEG sensors and not on system construction concerns, it should be noted that a practical implementation of an OPM-based osMEG system, such as the one described here, warrants addressing some of the potential limitations of the technology. While sensor movements relative to the head (and the associated artifacts) are minimal in an osMEG system with an individualized cap or head-shape-adjustable helmet, the sensors moving within any remnant magnetic field in the shielded room causes measurement artifacts. Dynamic active shielding can however reduce the remnant field to minimize such movement artifacts, and ensure the sensors stay within dynamic range and suppress cross-axis projection errors (Seymour et al., 2022; Robinson et al., 2020), and synthetic gradiometry and homogeneous field correction can further help tackle environmental interference (Seymour et al., 2022, Robinson et al., 2020). Heat generated by OPM-based osMEG systems may also become an issue in large systems, such as the one described here, and may require an active cooling system. Supporting structures (helmet or sensors adapters for a cap) in a densely populated system such as a 128-sensor OPM system – especially an OPM-EEG combination – would further need to be carefully designed to accommodate all the sensors in addition to providing sufficient air flow for cooling. Heat is however mainly a concern for today's alkali-based OPMs, and other sensors variants, such as helium4-based OPMs, require no heating and thus have a lower risk of causing thermal discomfort (Fourcault et al., 2021).

In conclusion, our results demonstrate that osMEG sensors can detect and localize initial low-voltage, high-frequency seizure activity with superior sensitivity and accuracy, thereby enabling significantly improved non-invasive SOZ localization at a level that cannot be achieved by other non-invasive clinical neurophysiological modalities such as convMEG or EEG. OsMEG measurements thus holds the promise of significantly improving sEEG implantation accuracy, and thereby improving epilepsy surgery outcome and safety. Practical measurements are of course needed to confirm our results and to demonstrate the usefulness of osMEG to neurosurgeons in a clinical setting. On that note, a 128-channel OPM-based osMEG system will be installed at Karolinska Institute, National Facility for Magnetoencephalography (<https://www.natmeg.se>) during early spring 2024, and our group is accordingly preparing to follow up these modeling results with osMEG recordings on epilepsy patients, to explore the clinical potential of osMEG further.

Funding

This research did not receive any specific grant from funding agencies in the public, commercial, or not-for-profit sectors.

Conflict of interest statement

None of the authors have potential conflicts of interest to be disclosed.

Appendix A. Supplementary material

Supplementary Figs. 4A–4C, 5–6 demonstrate on scalp MEG (osMEG), conventional MEG (convMEG) and EEG from six additional epileptic networks (please see article Fig. 2 for the anatomical localization, extent and naming convention of these networks) analyzed in the study. Supplementary Figs. 4A–4C (all filtered 1–130 Hz using a one-pass, zero-phase non-casual time-domain

finite impulse filter) show osMEG raw sensor data visibility of low-amplitude, high-frequency (100 Hz) initial ictal activity alongside spectral power upregulation at the ictal onset (time 3 second; please see article Fig. 2 for overview of the spatiotemporal development of the simulated seizure activity). In comparison, Supplementary Figs. 5 and 6 demonstrate the first seizure activity detected (visually and using time-frequency analysis) by convMEG (Supplementary Fig. 5) and by EEG (Supplementary Fig. 6) at time 15 seconds (please see article Fig. 2 for overview of the spatiotemporal development of simulated seizure activity). Supplementary material to this article can be found online at <https://doi.org/10.1016/j.clinph.2023.10.006>.

References

- Alkawadri R, Burgess RC, Kakisaka Y, Mosher JC, Alexopoulos AV. Assessment of the utility of ictal magnetoencephalography in the localization of the epileptic seizure onset zone. *JAMA Neurol* 2018;75:1264–72. <https://doi.org/10.1001/jamaneurol.2018.1430>.
- Blume WT, Ociepa D, Kander V. Frontal lobe seizure propagation: Scalp and subdural EEG studies. *Epilepsia* 2001;42:491–503. <https://doi.org/10.1046/j.1528-1157.2001.26700.x>.
- Boto E, Bowtell R, Krüger P, Fromhold TM, Morris PG, Meyer SS, et al. On the potential of a new generation of magnetometers for MEG: A beamformer simulation study. *PLoS One* 2016;11. <https://doi.org/10.1371/journal.pone.0157655>.
- Boto E, Hill RM, Rea M, Holmes N, Seedat ZA, Leggett J, et al. Measuring functional connectivity with wearable MEG. *Neuroimage* 2021;230. 117815. <https://doi.org/10.1016/j.neuroimage.2021.117815>.
- Boto E, Holmes N, Leggett J, Roberts G, Shah V, Meyer SS, et al. Moving magnetoencephalography towards real-world applications with a wearable system. *Nature* 2018;555:657–61. <https://doi.org/10.1038/nature26147>.
- Dale AM, Fischl B, Sereno MI. Cortical surface-based analysis I. Segmentation and surface reconstruction. *Neuroimage* 1999;9:179–94. <https://doi.org/10.1006/nimg.1998.0395>.
- Duez L, Beniczky S, Tankisi H, Hansen PO, Sidenius P, Sabers A, et al. Added diagnostic value of magnetoencephalography (MEG) in patients suspected for epilepsy, where previous, extensive EEG workup was unrevealing. *Clin Neurophysiol* 2016;127:3301–5. <https://doi.org/10.1016/j.clinph.2016.08.006>.
- Duez L, Tankisi H, Hansen PO, Sidenius P, Sabers A, Pinborg LH, et al. Electromagnetic source imaging in presurgical workup of patients with epilepsy: A prospective study. *Neurology* 2019;92:e576–86. <https://doi.org/10.1212/WNL.0000000000006877>.
- Engel JJ. Mesial temporal lobe epilepsy: What have we learned? *Neuroscientist* 2001;7:340–52. <https://doi.org/10.1177/107385840100700410>.
- Fischl B, Sereno MI, Dale AM. Cortical surface-based analysis: II. Inflation, flattening, and a surface-based coordinate system. *Neuroimage* 1999;9:195–207. <https://doi.org/10.1006/nimg.1998.0396>.
- Fourcault W, Romain R, Le Gal G, Bertrand F, Josselin V, Le Prado M, et al. Helium-4 magnetometers for room-temperature biomedical imaging: toward collective operation and photon-noise limited sensitivity. *Opt Express* 2021;29:14467–75. <https://doi.org/10.1364/oe.420031>.
- Gramfort A, Luessi M, Larson E, Engemann DA, Strohmeier D, Brodbeck C, et al. MEG and EEG data analysis with MNE-Python. *Front Neurosci* 2013;7:1–13. <https://doi.org/10.3389/fnins.2013.00267>.
- Hari R, Baillet S, Barnes G, Burgess R, Forss N, Gross J, et al. IFCN-endorsed practical guidelines for clinical magnetoencephalography (MEG). *Clin Neurophysiol* 2018;129:1720–47. <https://doi.org/10.1016/j.clinph.2018.03.042>.
- Heiden C. SQUID and SQUID system developments for biomagnetic applications. *Clin Phys Physiol Meas* 1991;12(Suppl B):67–73. <https://doi.org/10.1088/0143-0815/12/B/009>.
- Hill RM, Boto E, Rea M, Holmes N, Leggett J, Coles LA, et al. Multi-channel whole-head OPM-MEG: Helmet design and a comparison with a conventional system. *Neuroimage* 2020;219. <https://doi.org/10.1016/j.neuroimage.2020.116995>.
- Hunold A, Funke ME, Eichardt R, Stenroos M, Hauelsen J. EEG and MEG: Sensitivity to epileptic spike activity as function of source orientation and depth. *Physiol Meas* 2016;37:1146–62. <https://doi.org/10.1088/0967-3334/37/7/1146>.
- Iivanainen J, Stenroos M, Parkkonen L. Measuring MEG closer to the brain: Performance of on-scalp sensor arrays. *Neuroimage* 2017;147:542–53. <https://doi.org/10.1016/j.neuroimage.2016.12.048>.
- Iwasaki M, Pestana E, Burgess RC, Lüders HO, Shamoto H, Nakasato N. Detection of epileptiform activity by human interpreters: blinded comparison between electroencephalography and magnetoencephalography. *Epilepsia* 2005;46:59–68.
- Jayakar P, Dunoyer C, Dean P, Ragheb J, Resnick T, Morrison G, et al. Epilepsy surgery in patients with normal or nonfocal MRI scans: Integrative strategies offer long-term seizure relief. *Epilepsia* 2008;49:758–64. <https://doi.org/10.1111/j.1528-1167.2007.01428.x>.
- Jayakar P, Gaillard WD, Tripathi M, Libenson MH, Mathern GW, Cross JH. Diagnostic test utilization in evaluation for resective epilepsy surgery in children. *Epilepsia* 2014;55:507–18. <https://doi.org/10.1111/epi.12544>.
- Jayakar P, Gotman J, Harvey AS, Palmmini A, Tassi L, Schomer D, et al. Diagnostic utility of invasive EEG for epilepsy surgery: Indications, modalities, and techniques. *Epilepsia* 2016;57:1735–47. <https://doi.org/10.1111/epi.13515>.
- Kane N, Acharya J, Beniczky S, Caboclo L, Finnigan S, Kaplan PW, et al. A revised glossary of terms most commonly used by clinical electroencephalographers and updated proposal for the report format of the EEG findings. *Revision 2017. Clin Neurophysiol Pract* 2017;2:170–85. <https://doi.org/10.1016/j.cnp.2017.07.002>.
- Kanno A, Nakasato N, Oogane M, Fujiwara K, Nakano T, Arimoto T, et al. Scalp attached tangential magnetoencephalography using tunnel magneto-resistive sensors. *Sci Rep* 2022;12:6106. <https://doi.org/10.1038/s41598-022-10155-6>.
- Kellinghaus C, Lüders HO. Frontal lobe epilepsy. *Epileptic Disord* 2004;6:223–39.
- Komssi S, Huttunen J, Aronen HJ, Ilmoniemi RJ. EEG minimum-norm estimation compared with MEG dipole fitting in the localization of somatosensory sources at S1. *Clin Neurophysiol* 2004;115:534–42. <https://doi.org/10.1016/j.clinph.2003.10.034>.
- Koshev N, Butorina A, Skidchenko E, Kuzmichev A, Ossadtchi A, Ostras M, et al. Evolution of MEG: A first MEG-feasible fluxgate magnetometer. *Hum Brain Mapp* 2021;42:4844–56. <https://doi.org/10.1002/hbm.25582>.
- Kwan P, Brodie MJ, Kälviäinen R, Yurkewicz L, Weaver J, Knapp LE. Long-term outcome after epilepsy surgery: Relapsing, remitting disorder? *Epilepsy Curr* 2012. <https://doi.org/10.5698/1535-7511-12.4.12610.1056/NEJMra1004418>.
- Medvedovsky M, Taulu S, Gaily E, Metsähonkala EL, Mäkelä JP, Ekstein D, et al. Sensitivity and specificity of seizure-onset zone estimation by ictal magnetoencephalography. *Epilepsia* 2012;53:1649–57. <https://doi.org/10.1111/j.1528-1167.2012.03574.x>.
- Murakami S, Okada Y. Invariance in current dipole moment density across brain structures and species: Physiological constraint for neuroimaging. *Neuroimage* 2015;111:49–58. <https://doi.org/10.1016/j.physbeh.2017.03.040>.
- Oishi M, Otsubo H, Kameyama S, Morota N, Masuda H, Kitayama M, et al. Epileptic spikes: Magnetoencephalography versus simultaneous electrocorticography. *Epilepsia* 2002;43:1390–5. <https://doi.org/10.1046/j.1528-1157.2002.10702.x>.
- Olmi S, Petkoski S, Guye M, Bartolomei F, Jirsa V. Controlling seizure propagation in large-scale brain networks. *PLoS Comput Biol* 2019;15. <https://doi.org/10.1371/journal.pcbi.1006805>.
- Osborne J, Orton J, Alem O, Shah V. Fully integrated, standalone zero field optically pumped magnetometer for biomagnetism. *Proc SPIE* 2018. <https://doi.org/10.1117/12.2299197>.
- Pfeiffer C, Ruffieux S, Jonsson L, Chukharkin ML, Kalabukhov A, Xie M, et al. A 7-channel high-Tc SQUID-based on-scalp MEG system. *IEEE Trans Biomed Eng* 2020;67:1483–9. <https://doi.org/10.1109/tbme.2019.2938688>.
- Park HM, Nakasato N, Iwasaki M, Shamoto H, Tominaga T, Yoshimoto T. Comparison of magnetoencephalographic spikes with and without concurrent electroencephalographic spike in extra temporal epilepsy. *Tohoku J Exp Med* 2004;203:165–74.
- Park HM, Nakasato N, Iwasaki M, Shamoto H, Yoshimoto T. In: Nowak H, Hauelsen J, Giessler F, Huonker R, editors. Proceedings of the 13th international conference on biomagnetism. Berlin: VDE Verlag GMBH; 2002. p. 260–2.
- Plummer C, Vogrin SJ, Woods WP, Murphy MA, Cook MJ, Liley DTJ. Interictal and ictal source localization for epilepsy surgery using high-density EEG with MEG: A prospective long-term study. *Brain* 2019;142:932–51. <https://doi.org/10.1093/brain/awz015>.
- Proix T, Jirsa VK, Bartolomei F, Guye M, Truccolo W. Predicting the spatiotemporal diversity of seizure propagation and termination in human focal epilepsy. *Nat Commun* 2018;9. <https://doi.org/10.1038/s41467-018-02973-v>.
- Rampf S, Stefan H, Wu X, Kaltenhäuser M, Maess B, Schmitt FC, et al. Magnetoencephalography for epileptic focus localization in a series of 1000 cases. *Brain* 2019;142:3059–71. <https://doi.org/10.1093/brain/bhw393>.
- Riaz B, Pfeiffer C, Schneiderman JF. Evaluation of realistic layouts for next generation on-scalp MEG: Spatial information density maps. *Sci Rep* 2017;7. <https://doi.org/10.1038/s41598-017-07046-6>.
- Robinson SE, Andonegui AB, Holroyd T, Hughes KJ, Alem O, Knappe S, et al. Cross-axis dynamic field compensation of optically pumped magnetometer arrays for MEG. *Neuroimage* 2020;262. 119559. <https://doi.org/10.1016/j.neuroimage.2022.119559>.
- Ryynänen O, Hyttinen J, Malmivuo J. Study on the spatial resolution of EEG - effect of electrode density and measurement noise. In: The 26th annual international conference of the IEEE Engineering in Medicine and Biology Society, San Francisco, CA, USA, p. 4409–12. <https://doi.org/10.1109/EMBS.2004.1404226>.
- Sarvas J. Basic mathematical and electromagnetic concepts of the biomagnetic inverse problem. *Phys Med Biol* 1987;32:11–22. <https://doi.org/10.1088/0031-9155/32/1/004>.
- Schneiderman JF. Information content with low- vs. high-T(c) SQUID arrays in MEG recordings: The case for high-T(c) SQUID-based MEG. *J Neurosci Methods* 2014;222:42–6. <https://doi.org/10.1016/j.neumeth.2013.10.007>.
- Seymour RA, Alexander N, Mellor S, O'Neill GC, Tierney TM, Barnes GR, et al. Interference suppression techniques for OPM-based MEG: Opportunities and challenges. *Neuroimage* 2022;247. 118834. <https://doi.org/10.1016/j.neuroimage.2021.118834>.

- Stefan H, da Silva FHL. Epileptic neuronal networks: Methods of identification and clinical relevance. *Front Neurol* 2013;4:8. <https://doi.org/10.3389/fneur.2013.00008>.
- Tatum WO. Mesial temporal lobe epilepsy. *J Clin Neurophysiol* 2012;29:356–65. <https://doi.org/10.1097/WNP.0b013e31826b3ab7>.
- Taulu S, Simola J. Spatiotemporal signal space separation method for rejecting nearby interference in MEG measurements. *Phys Med Biol* 2006;51:1759–68. <https://doi.org/10.1088/0031-9155/51/7/008>.
- De Tiège X, Carrette E, Legros B, Vonck K, Op De Beeck M, Bourguignon M, et al. Clinical added value of magnetic source imaging in the presurgical evaluation of refractory focal epilepsy. *J Neurol Neurosurg Psychiatry* 2012;83:417–23. <https://doi.org/10.1136/jnnp-2011-301166>.
- De Tiège X, Lundqvist D, Beniczky S, Seri S, Paetau R. Current clinical magnetoencephalography practice across Europe: Are we closer to use MEG as an established clinical tool? *Seizure* 2017;50:53–9. <https://doi.org/10.1016/j.seizure.2017.06.002>.
- Toth M, Papp KS, Gede N, Farkas K, Kovacs S, Isnard J, et al. Surgical outcomes related to invasive EEG monitoring with subdural grids or depth electrodes in adults: A systematic review and meta-analysis. *Seizure* 2019;70:12–9. <https://doi.org/10.1016/j.seizure.2019.06.022>.
- Wendling F, Bartolomei F, Bellanger JJ, Chauvel P. Epileptic fast activity can be explained by a model of impaired GABAergic dendritic inhibition. *Eur J Neurosci* 2002;15:1499–508. <https://doi.org/10.1046/j.1460-9568.2002.01985.x>.
- Wendling F, Benquet P, Bartolomei F, Jirsa V. Computational models of epileptiform activity. *J Neurosci Methods* 2016;260:233–51. <https://doi.org/10.1016/j.jneumeth.2015.03.027>.
- Westin K, Pfeiffer C, Andersen LM, Ruffieux S, Cooray G, Kalaboukhov A, et al. Detection of interictal epileptiform discharges: A comparison of on-scalp MEG and conventional MEG measurements. *Clin Neurophysiol* 2020;131:1711–20. <https://doi.org/10.1016/j.clinph.2020.03.041>.
- Xie M, Schneiderman JF, Chukharkin ML, Kalaboukhov A, Whitmarsh S, Lundqvist D, et al. High-Tc SQUID vs. low-Tc SQUID-based recordings on a head phantom: Benchmarking for magnetoencephalography. *IEEE Trans Appl Supercond* 2015;25. <https://doi.org/10.1109/TASC.2014.2366420>.